Astronomy & Astrophysics manuscript no. argus
February 1, 2008
© ESO 2008

arXiv:0708.4134v1 [astro-ph] 30 Aug 2007

LETTER TO THE EDITOR

Star-gas decoupling and a non-rotating stellar core in He 2-10

Integral field spectroscopy with FLAMES/ARGUS⋆

T. Marquart[1], K. Fathi[2,3], G. Östlin[3], N. Bergvall[1], R. J. Cumming[3], and P. Amram[4]

[1] Department of Astronomy and Space Physics, Box 515, SE-75120 Uppsala, Sweden
e-mail: thomas.marquart@astro.uu.se
[2] Instituto de Astrofí sica de Canarias, C/ Ví a Láctea s/n, 38200 La Laguna, Tenerife, Spain
[3] Stockholm Observatory, AlbaNova University Center, SE-106 91 Stockholm, Sweden
[4] Observatoire Astronomique Marseille-Provence, Laboratoire d'Astrophysique de Marseille UMR 6110, 2 place Le Verrier, F-13248 Marseille Cedex 4, France

Received; June 22, 2007

ABSTRACT

Aims. We study the two-dimensional distribution and kinematics of the stellar and gaseous components in the centre of the prototype Wolf-Rayet blue compact dwarf galaxy, He 2-10. The aim is to compare the kinematics of gas and stars in order to determine whether they are consistent with one another, or if stars and gas can be decoupled due to gravitational perturbations and feedback from star formation.

Methods. We have used the integral field unit ARGUS, part of FLAMES on the European Southern Observatory's Very Large Telescope, to target the Ca II $\lambda\lambda 8498, 8542, 8662$ Å triplet in the central 300×480 parsecs of He 2-10. The selected wavelength regime includes several prominent spectral features, including the Paschen series and the [S III] emission-line, which we have used to derive the kinematics of the ionised interstellar medium.

Results. We find no systematic trend in the velocities of the stars over the observed field of view and conclude that the stellar kinematics is governed by random motions. This is in contrast to the motions the ionised interstellar medium, where we find spatial velocity variations up to 60 km s^{-1}. Our gas velocity field is consistent with previous studies of both the molecular gas and the feedback-driven outflow in He 2-10. We interpret the kinematic decoupling between the stars and the gas as He 2-10 being in the process of transformation to a dwarf elliptical galaxy.

Key words. Galaxies: dwarf – Galaxies: kinematics and dynamics – Galaxies: starburst – Galaxies: individual (He 2-10)

1. Introduction

Blue compact galaxies (BCGs) are important laboratories for testing existing theories for dwarf galaxy formation and evolution. This is because many of them form stars at rates that are unsustainable over long periods and because of their low interstellar medium (ISM) metallicities. The large amounts of young stars in BCGs give rise to a blue continuum and strong emission-lines, dominating the optical light. Their high star formation rates, high gas content, chaotic morphology and low metallicities make them often being regarded as local counterparts of young galaxies (e.g., Kunth & Östlin 2000). However, detection of faint old stellar populations suggests that these systems are intrinsically old, even in the most youthful cases (Östlin & Mouhcine 2005). The puzzle of what triggers starbursts in BCGs remains unsolved, although merger events are likely to play an important role.

Previously, Fabry-Perot interferometric studies of the Hα line (Östlin et al. 1999, 2001) have revealed disturbed kinematics, indicating dwarf galaxy mergers as a likely explanation for the formation of BCGs. Despite local turbulence, the Hα kinematics nevertheless suggest overall gravitational support. Due to the ubiquitous presence of shocks, supernova winds and heating by massive stars, it is unclear if the ISM follows the motions of the stars, which are bound to follow the gravitational potential. Both mass estimates from gas kinematics and evolutionary scenarios based on the assumption that BCGs are self-gravitating may therefore be uncertain. This is of importance not only for the local universe, but also at higher redshift, where strong emission-lines are often the only usable kinematical tracers. Thus, mass estimates of high-redshift star-forming galaxies may change significantly if the stars and gas display different kinematics.

Stellar motions are usually studied using optical absorption lines. However, in BCGs, where metallicities are low and star formation is strong, the absorption lines become easily diluted by the strong blue continuum of hot stars and the nebular emission. In the near-infrared, the Ca II $\lambda\lambda 8498, 8542, 8662$ Å triplet (hereafter Ca triplet) can be used to derive reliable stellar kinematic information (Dressler 1984). In a previous study using Very Large Telescope (VLT) long-slit spectroscopy, we confirmed on ESO 400-G43 that the Ca triplet can be used to probe the stellar kinematics in BCGs (Östlin et al. 2004). Our study showed that the stellar component did not show the super-keplerian decline observed for the ionised gas. Thus, stars can be kinematically decoupled from the gas. With the help of integral field units (IFUs), we can compare the gaseous and stellar motions by spectroscopy in two spatial dimensions.

Send offprint requests to: T. Marquart

⋆ Based on observations collected at the European Southern Observatory, Paranal, Chile, under observing programme 74.B-0771.

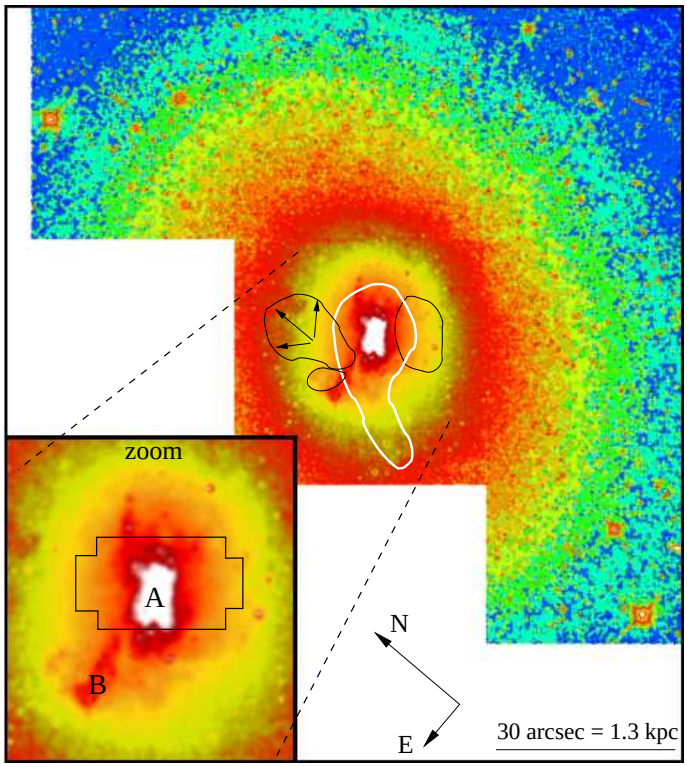

Fig. 1. HST/WFPC2 F814W archival image of He 2-10 with an overlaid CO (thick white) contour from (Kobulnicky et al. 1995). The thin black lines outline the positions of bubbles observed in Hα emission (Méndez et al. 1999). The inset shows the central region at larger scale together with the footprint of our ARGUS observations and regions A and B, as discussed in the text.

Here, we present results from IFU observations of the central 300×480 parsecs in He 2-10, targeting the Ca triplet. He 2-10 is a well-known BCG with an absolute *B*-band magnitude of −19 and two prominent star-forming regions (see Fig 1). The super star clusters (SSCs) in the central region (region A) have an age of 4-5 Myr (Chandar et al. 2003) while those in region B, lying east of the centre, are older. It has been argued by Méndez et al. (1999) that strong feedback from star formation drives a bipolar outflow in He 2-10. The systemic velocity of 870 km s^{-1} is too low to serve as a good distance measure because it cannot be assumed to belong to the Hubble flow, due to the influence of the Virgo cluster. Here, we adopt the distance of 9 Mpc used by Kobulnicky et al. (1995), corresponding to a physical scale of 46.3 pc arcsec^{-1}.

2. Observations and Data Reduction

The observations were carried out under good weather conditions during two nights in November 2004 with FLAMES at European Southern Observatory's VLT (VLT/UT2) and its IFU, ARGUS, connected to the spectrograph GIRAFFE (Pasquini et al. 2002). The coarse (1:1) scale of ARGUS gives a spatial resolution of 0.″52 pix ≈ 30 pc/pix and the 22 × 14 pixels result in a field-of-view of 11.″4 × 7.″3 placed with 40° position angle on region A in He 2-10 (see Fig 1). The light from each resolution element is fibre-fed to the spectrograph where spectra with $R \approx 10400$ ranging from 8200 Å to 9380 Å were measured. The spectra therefore cover the Ca triplet, O I λ8446, [Cl II] λ8579, [Fe III] λ8617, [S III] λ9069[1], and the Paschen 9 to Paschen 19 emission-lines of H I.

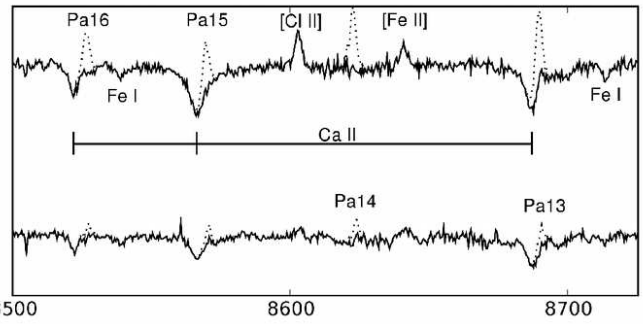

Fig. 2. Example of two spectra from single fibres with different S/N. Dotted line: original spectrum. Solid line: after subtraction of the Paschen lines.

To save overhead time, we used fast target acquisition, thereby trusting the pointing accuracy of the telescope. Four frames were obtained with a total exposure time of 3.2 hours. The data were reduced using the software and methods by Piskunov & Valenti (2002), with reduction steps including standard techniques for bias subtraction, flat-fielding, wavelength calibration and optimised extraction of each spectrum. The background emission from the sky was then subtracted using the simultaneously observed spectra from the 15 sky fibres located at a large distance around the target (see Kaufer et al. 2003, for details).

Since all three lines of the Ca triplet have Paschen emission lines superimposed on their red wings, it is crucial to accurately subtract the emission features before deriving the stellar kinematics. By fitting several isolated Paschen lines simultaneously and using the theoretical relative line-strengths, we subtracted a model spectrum for Paschen emission for each pixel. The model spectrum was constructed by fitting the uncontaminated lines of Paschen 9, 10, 14, 17, 18, and 19. Manual adjustments were made in cases where the signal was too low to get a reliable model for the Paschen lines. Fig. 2 shows two examples of subtracted and unsubtracted spectra in the region around the Ca triplet. Both emission and absorption lines are indicated.

We parametrise the stellar line-of-sight velocity distribution by a Gaussian profile using the penalized pixel fitting algorithm developed by Cappellari & Emsellem (2004) together with a selection of template stars from the stellar library by Cenarro et al. (2001). Using this technique, we derived the kinematics using the best linear combination of 18 carefully chosen template stars covering M6 V with $T_{\rm eff}$=3721 to O9 V with $T_{\rm eff}$=36300 K, and metallicities ranging between -2.25 and 0.13 solar. The stellar types used were K0 V, A8 Vn, K0 III, K3 IIb, K4 Iab, M3 II-III, K3 Iab, 09 V, B5, K3 III, A4, K0 V, M6 V, M2 V, G5 IIIw, K7 V, F0 and M4 V. Thus our derived kinematics is not affected by template mismatching effects, since a different combination of stellar template spectra is compiled for each individual spectrum. To match the template stellar library, we degraded the spectral resolution of our data from 0.2 Å/pix to 0.85 Å/pix. This simultaneously increased the signal in the fainter pixels, while still resolving the Ca triplet well enough to derive the

[1] The rest-wavelength of this [S III] line is only determined to 0.5 Å (Ralchenko et al. 2007), corresponding to 16.5 km s^{-1}. Throughout this paper, we adopt 9069.0 Å.

kinematics accurately. However, for fitting the emission lines, we used the full-resolution spectra.

Although the pixel fitting routine delivers formal errors, these could be underestimated since this formalism suppresses the noise in the observations. We used Monte Carlo simulations to calculate more realistic error estimates. For each pixel, we derived the kinematics for 250 realisations, i.e., Gaussian randomised error-spectra added to the galaxy spectra. We found that the average error over all pixels is 6 km s^{-1} for the velocities, and 9 km s^{-1} for the stellar velocity dispersions. We estimate that the emission line kinematics can be derived within the same level of uncertainty or better.

In order to test the robustness of the derived stellar kinematics, we were able to reproduce the stellar velocity field independently by instead cross-correlating with three template stars of different type (K0II, K0III, G8Iab) that were observed in the same nights with the same instrumental setup. To quantify the systematic error from the subtraction of the Paschen emission, we varied the strength of the subtraction from twice the adopted amount to no subtraction at all. The goodness of the subsequent fitting confirmed that the subtraction is optimal within 20%. This corresponds to a possible systematic error of 10 and 15 km s^{-1} for the stellar velocities and line widths, respectively. However, this is probably quite conservative since there is no indication that this error acts always towards under- or oversubtraction and the spread in stellar velocity values over the whole field is only 8 km s^{-1}.

3. Results and Discussion

3.1. Stars

The Ca triplet is one of the most prominent near-infrared features of cool stars. Although it originates mainly from red giant and supergiant stars, it is present in stars of types A to M. Because the light from the galaxy is dominated by the bright and young SSCs (Johnson et al. 2000), it is not the presumably relaxed old underlying stellar population that is sampled when observing the Ca triplet, but instead fairly young stars — red supergiants appear after 5 Myr — that have been formed during the current burst of star formation. This is consistent with the fact that we do not see any evidence for absorption in the Paschen lines (cf. Fig. 2).

The stellar velocity field (panel (c) in Fig. 3) displays no significant velocity gradient across the field, and thereby no sign of rotation. We find the stellar component of He 2-10 to have a systemic velocity of 872 ± 6 km s^{-1}, in good agreement with the usually adopted systemic velocity for He 2-10 (e.g., Johansson 1987). The absence of a gradient in the stellar velocity field suggests that the young component, which dominates the light, is relaxed and governed by random motions. The stellar velocity dispersion map (panel (d)) shows an average value of 45 ± 4 km s^{-1} outside the bright starburst centre (region A), while in the very centre itself the stellar velocity dispersion drops to 28 ± 3 km s^{-1}. This can be understood by assuming that the young stars, dominating the light, are being formed in a locally dense and dynamically less hot environment. Outside the burst region, the stars are older and have had more time to virialize with the starburst host, thereby increasing the velocity dispersion.

Assuming virialisation, we can estimate masses using the relation $M_\sigma = 1.1 \times 10^6 \cdot r_e \cdot \sigma^2$, where the effective radius r_e is given in units of kpc, σ in km s^{-1}, and M_σ in $M_\odot$ (Bender et al. 1992; Guzman et al. 1996). For the central starburst with a size of $\approx 1.1''$ (derived from archival Hubble Space Telescope NICMOS camera H-band photometry) and $\sigma = 28$ km s^{-1}, we calculate the mass to be $4 \times 10^7 M_\odot$. The same exercise for the region outside region A, represented by an effective radius of $\approx 6''$ and the average stellar velocity dispersion $\sigma = 45$ km s^{-1} gives a total galaxy mass of $6 \times 10^8 M_\odot$. This compares very well with the total mass in atomic and molecular gas measured by Kobulnicky et al. (1995). The irregular structure of the central morphology and possible variations in the mass to light ratio leads to an uncertainty in r_e of about a factor of 2, translating linearly to the derived mass. By integrating the light profiles from Noeske et al. (2003), we estimate a mass-to-light ratio in the H band of 0.05 and 0.2 for the two masses derived above, respectively. This is consistent with the very young stellar population in He 2-10.

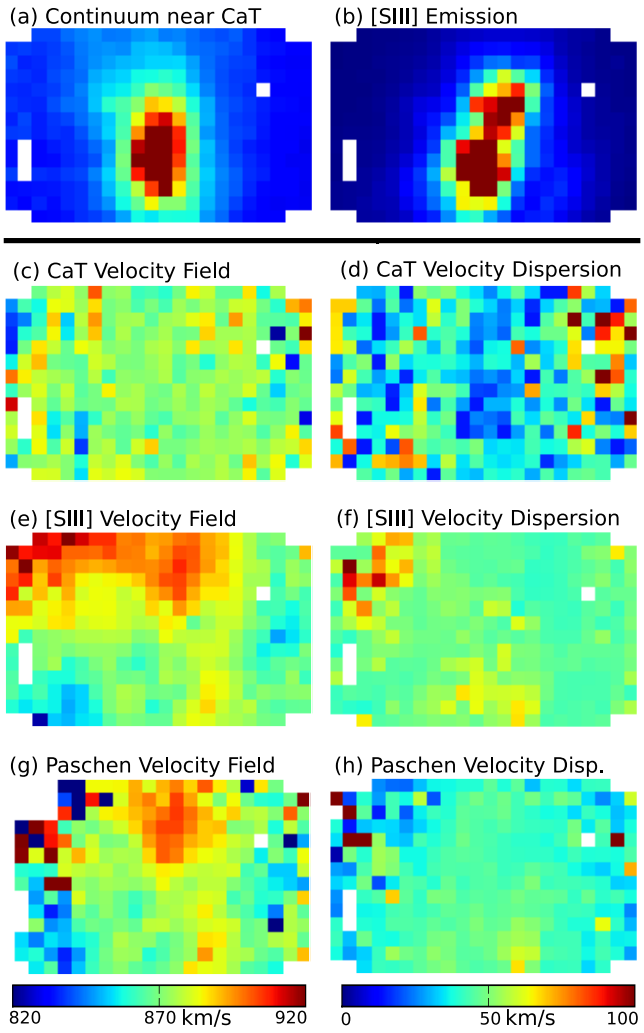

Fig. 3. Panels showing the field of view of ARGUS, 22 by 14 pixels, corresponding to $11\farcs4 \times 7\farcs3$. As indicated in Fig. 1, left is north-east and up is north-west. Panels (a) and (b) show the continuum emission near the Ca triplet and the monochromatic emission from [S III] respectively, in arbitrary flux units. Panels (c) and (d): Heliocentric line-of-sight velocity and velocity dispersion from the Ca triplet. Colours for these and the following panels indicate values according to the colour bars beloweach column. Panels (e) and (f): Velocity and velocity dispersion from [S III]. Panels (g) and (h): Velocity and velocity dispersion from the Paschen lines.

3.2. Gas

The emission-line velocity dispersions of the [S III] and Paschen emission-lines are almost constant over the field of view, with average values 49 ± 6 (standard deviation) and 44 ± 3 km s^{-1}, respectively. In the northern corner of the field, there is an indication of an increase in σ for the [S III] and a decrease for the Paschen lines, although this is the region with the weakest signal. Overall, these values are higher than the stellar velocity dispersion at the very centre, but they agree with the value outside the starburst region. The observed gaseous velocity dispersion is more than a factor two higher than the average measured turbulent velocity dispersion of H II regions in spiral galaxies (e.g., Chu & Kennicutt 1994) but not unusually high for a BCG where it is often used empirically as a mass measure (e.g., Melnick et al. 1987; Guzman et al. 1996; Östlin et al. 2001). Since the gas velocity dispersion in He 2-10 is higher than that of the stars in the centre, the outflow (see below) probably also contributes to the line width.

The velocity fields of the [S III] and Paschen emission-lines (panels (e) and (g) in Fig. 3) clearly deviate from that of the stars. We observe gas velocities to be generally higher than the stellar velocity and find the region west and north-west of the central starburst to display velocities reaching up to 50 km s^{-1} higher than the systemic velocity. At the east and south-east, the [S III] line-of-sight velocity is less than the systemic value by 10 km s^{-1}. Except in regions with barely detected Paschen emission, the velocity field of the [S III] line resembles that of the Paschen lines, in agreement with Hα velocities measured by Méndez et al. (1999) in the sense that we observe blueshifted lines towards the north-east of the field. We also find agreement with our Hα Fabry-Perot measurements (Marquart et al. 2006, and 2007 in preparation).

Although on larger scales, the gas in He 2-10 is known to rotate (Kobulnicky et al. 1995; Marquart et al. 2006), the emission-line velocity fields we observe here alone cannot establish whether the high and low values to either side of the zero-velocity curve are signatures of rotation in the centre of He 2-10. The rough orientation of the velocity gradient with the morphological major axis might suggest this, but the corresponding mass from assuming Keplerian motions is an order of magnitude below the value derived above. In addition, the lack of rotation in the stellar component seems to preclude the existence of a dominant star-forming disk. Kobulnicky et al. (1995) find an elongated cloud of molecular gas with a tail towards the south-east (see also our Fig. 1). Over the region of our field of view, the CO gas displays a velocity gradient that is in agreement with the gaseous motions presented here. Since the stars do not follow these motions, they probably have not formed out of the same gas, which might instead represent the part of the cloud with high angular momentum or the infall of fresh gas.

On the other hand, the ISM is subject to strong feedback from the starburst that drives the well-studied outflow in He 2-10. Both Beck & Kovo (1999) and Méndez et al. (1999) have observed bubble structures in deep Hα images (cf. Fig. 1) blowing out towards the north-east and south-west of the central starburst. Johnson et al. (2000) find this scenario to be consistent with the measured energy output from the SSCs in the central starburst. We measure blueshifted lines towards the proposed outflow regions on both sides that can be attributed to a bipolar outflow, seen close to edge-on.

Schwartz et al. (2006) have used ultraviolet (UV) absorption lines to measure the speed of the outflow at the position of the brightest SSCs and found it to be −170 km s^{-1} with respect to the systemic velocity. In contrast to this, we measure gaseous velocities at the systemic value. We attribute this discrepancy to the different regions probed. UV absorption lines sample the cold and warm ISM in the foreground, while emission lines trace the ionised ISM at the location of the starbrust.

4. Conclusions

We have used integral field spectroscopy to measure the stellar kinematics in He 2-10 using the Ca triplet absorption lines, and compared it with the motions of the ionised gas. We find a large discrepancy between stars and gas. The stellar component shows no signatures of rotation or any other non-random motions. The gas, however, shows bulk motions that are consistent with previous results from molecular gas kinematics and the bipolar outflow, driven by the starburst in the centre.

In particular, IFU spectroscopy has allowed us to show that the stars in the centre show no sign of rotation along any direction and that gas and stars are kinematically clearly decoupled. The virialization of the stellar component is compatible with He 2-10 being an advanced merger because simulations show that virialization is quick and that the peak in star formation rate in a galaxy merging event coincides with the completion of the merger (e.g., Barnes & Hernquist 1992; Cox et al. 2006).

That the stellar component is supported by velocity dispersion rather than rotation also hints toward the future evolution of He 2-10 in the direction of an elliptical-like galaxy (Geha et al. 2002), as earlier suggested by Koo et al. (1995) for more distant emission line galaxies. Indeed, the strongly peaked light profile will probably, after the burst has faded, resemble that of a nucleated dE like M 32 or NGC 205. The lower velocity dispersion that we find for the youngest stellar component in the very centre of He 2-10 may in time be dynamically heated and begin to resemble the rest of the galaxy.

Our results also suggest a need for caution in studies of starburst galaxies at higher redshifts, where emission-lines often are the only feasible kinematical tracers. Observed spatial variations in line-of-sight velocities need not be representative of the gravitational potential if decoupling between gas and stars is common.

Acknowledgements. T. Marquart wishes to thank Nikolai Piskunov for assisting in the data reduction. K.Fathi acknowledges support from the Instituto de Astrofísica de Canarias through project P3/86, the Royal Swedish Academy of Sciences' Hierta-Retzius foundation, and the Wenner-Gren Foundation. N. Bergvall and G. Östlin acknowledge support from the Swedish Research Council.

References

Barnes, J. E. & Hernquist, L. 1992, ARA&A, 30, 705
Beck, S. C. & Kovo, O. 1999, AJ, 117, 190
Bender, R., Burstein, D., & Faber, S. M. 1992, ApJ, 399, 462
Cappellari, M. & Emsellem, E. 2004, PASP, 116, 138
Cenarro, A. J., Cardiel, N., Gorgas, J., et al. 2001, MNRAS, 326, 959
Chandar, R., Leitherer, C., Tremonti, C., & Calzetti, D. 2003, ApJ, 586, 939
Chu, Y.-H. & Kennicutt, Jr., R. C. 1994, ApJ, 425, 720
Cox, T. J., Jonsson, P., Primack, J. R., & Somerville, R. S. 2006, MNRAS, 373, 1013
Dressler, A. 1984, ApJ, 286, 97
Geha, M., Guhathakurta, P., & van der Marel, R. P. 2002, AJ, 124, 3073
Guzman, R., Koo, D. C., Faber, S. M., et al. 1996, ApJ, 460, L5+
Johansson, L. 1987, A&A, 182, 179
Johnson, K. E., Leitherer, C., Vacca, W. D., & Conti, P. S. 2000, AJ, 120, 1273
Kaufer, A., Pasquini, L., Castillo, R., Schmutzer, R., & Smoker, J. 2003, The Messenger, 113, 15
Kobulnicky, H. A., Dickey, J. M., Sargent, A. I., Hogg, D. E., & Conti, P. S. 1995, AJ, 110, 116

Koo, D. C., Guzman, R., Faber, S. M., et al. 1995, ApJ, 440, L49
Kunth, D. & Östlin, G. 2000, A&A Rev., 10, 1
Marquart, T., Östlin, G., Bergvall, N., Amram, P., & Masegosa, J. 2006, in IAU Symposium, 235, 321
Melnick, J., Moles, M., Terlevich, R., & Garcia-Pelayo, J.-M. 1987, MNRAS, 226, 849
Méndez, D. I., Esteban, C., Filipović , M. D., et al. 1999, A&A, 349, 801
Noeske, K. G., Papaderos, P., Cairós, L. M., & Fricke, K. J. 2003, A&A, 410, 481
Östlin, G., Amram, P., Bergvall, N., et al. 2001, A&A, 374, 800
Östlin, G., Amram, P., Masegosa, J., Bergvall, N., & Boulesteix, J. 1999, A&AS, 137, 419
Östlin, G., Cumming, R. J., Amram, P., et al. 2004, A&A, 419, L43
Östlin, G. & Mouhcine, M. 2005, A&A, 433, 797
Pasquini, L., Avila, G., Blecha, A., et al. 2002, The Messenger, 110, 1
Piskunov, N. E. & Valenti, J. A. 2002, A&A, 385, 1095
Ralchenko, Y., Jou, F.-C., Kelleher, D., et al. 2007, NIST Atomic Spectra Database (version 3.1.2), [Online], National Institute of Standards and Technology, Gaithersburg, MD
Schwartz, C. M., Martin, C. L., Chandar, R., et al. 2006, ApJ, 646, 858

List of Objects

‘He 2-10’ on page 2